Available online at www.sciencedirect.com
SCIENCE DIRECT®
Journal of volcanology and geothermal research
ELSEVIER
Journal of Volcanology and Geothermal Research 131 (2004) 77–92
www.elsevier.com/locate/jvolgeores

Fissure eruption of flood basalts from statistical analysis of dyke fracture length

Daniel Mège [a,*], Tesfaye Korme [b]

[a] *Laboratoire de Tectonique, UMR CNRS 7072, Université Pierre et Marie Curie, Boîte 129, 4 place Jussieu, 75252 Paris Cedex 05, France*

[b] *Geology and Geophysics Department, Addis Ababa University, P.O. Box 81064, Addis Ababa, Ethiopia*

Received 14 September 2001; accepted 20 August 2003

Abstract

Flood basalt emplacement results from eruption of dyke swarms. Several lines of evidence suggest, however, that a large number of dykes in large igneous provinces have never erupted, or have done so over too short a length for any evidence of eruption to be found in the field. We have mapped 1025 dykes and dyke segments from two swarms in western Ethiopia, most of which are of basaltic composition, the others of silicic composition. The dykes cut across the basal breccia of the trap series, and are observed at a structural level c. 1000 m below the current top of the lava pile on the nearby volcanic plateau. We test the hypothesis that at such a depth, some of the basaltic dykes may have erupted whereas some others may not. Due to higher buoyancy within the trap series, silicic dykes are likely to have been systematically eruptive. The area is flat, which has allowed analysis of dyke length distribution at constant structural level, a useful approach for the characterisation of other fracture types such as tension fractures and faults. We found that dyke length follows a power-law distribution. When en échelon dyke segments are counted as single dykes (having as their length the accumulated length of the individual segments), the population exponent, 1.8, is in the mean of the exponents usually obtained for fracture data sets. This exponent correctly fits the shortest dykes considered (1–9 km). A much steeper slope (3.3) is obtained for the distribution of intermediate lengths (9–10 to 10–20 km), and is interpreted as a possible consequence of the eruption of those dominantly basaltic dykes that are more than 9–10 km long at the observed structural depth. The longest, silicic dykes (10–20 to 50 km) have the same population exponent as the shortest, basaltic dykes. This is explained by the homogeneous propagation mode of both populations, either dominantly horizontal or dominantly vertical. However, the silicic dyke population exhibits a slightly larger population coefficient, for which we discuss the possible influence of the Precambrian fabric. Analysis of fracture length distribution appears to be a promising tool for estimating how much of a dyke swarm is eruptive and better understanding the mechanisms of fissure eruption in large igneous provinces.

Keywords: dyke swarm; fracture population; fissure eruption; Ethiopian large igneous province

1. Introduction

Large igneous provinces (LIPs) are so systematically associated with dyke swarms (e.g., Ernst

* Corresponding author.
E-mail addresses: dmege@lgs.jussieu.fr (D. Mège), tkorme@yahoo.co.uk (T. Korme).

0377-0273/03/$ – see front matter © 2003 Elsevier B.V. All rights reserved.
doi:10.1016/S0377-0273(03)00317-2

and Buchan, 1997) that it is usually assumed that the lava flows are the result of fissure eruptions. Direct observation of a lava flow being fed by a dyke is, however, an exception. Field observation in LIPs of lava flows fed by dykes has been mainly documented for the Columbia River Basalts by Fuller (1927), Waters (1961), and in the key paper by Swanson et al. (1975), who identified linear vent systems at various stages of preservation and other evidence of dyke eruption. Such observations have been scarcely reported in other LIPs. One reason is that the Columbia River Basalts are the most recent (mainly 17–15.5 Ma, Reidel et al., 1989), least eroded, and most studied flood basalts. Another reason is that even though dykes may be observed to be in contact with the lava flows, magma withdrawal into a feeding fissure, or a resurgence of lava up the fissure after the flow has solidified, will break any connection that may have existed between the fissure and the flow (Waters, 1961). A third reason is that large surface areas covered by flood basalts appear to be totally exempt of dykes, owing to the distance lava flows can travel away from their vent (Tolan et al., 1989). Most of the Columbia River Province is exempt of dykes (e.g., Waters, 1961; Hooper, 1997), and a number of lava flows end hundreds of kilometres away from their vent. In the Ethiopian LIP, the Blue Nile gorges cut the northern volcanic plateau (Abyssinia) over hundreds of kilometres without any reported evidence of dyke exposures on the walls (Mohr, 1963).

How much dyke swarms feed LIP lavas is not clearly solved by geochemical data. While major and trace element abundances have allowed the linking of dykes and lava flows in the Columbia River Province (Fruchter and Baldwin, 1975), subtle chemical variations in the Precambrian Harp-Seal Lake flood basalt province in Canada appear to preclude direct lava flow feeding by most of the dyke swarm, an interpretation reinforced by the absence of dyke signatures on aeromagnetic data over the flood basalts (Cadman et al., 1994). In the Scoresby Sund in eastern Greenland, dykes associated with the North Atlantic Volcanic Province (Peulvast, 1991, and personal communication, 1994) are observed to stop in soft sedimentary layers below the lava pile. As far as we know from the literature, all the dykes reported in the swarms in LIPs are of mafic composition. The reason why most of them may not erupt in many instances, or may erupt over a

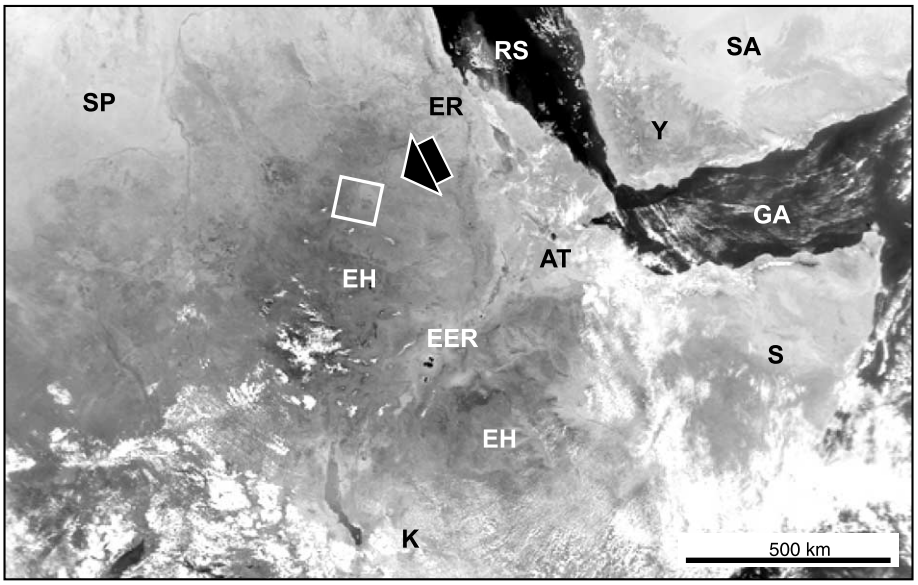

Fig. 1. Location of the study area. The box locates Fig. 3. AT: Afar triangle, EER: East Ethiopian rift, EH: Ethiopian volcanic highlands (Abyssinia and southeastern plateau, together making up the Ethiopian LIP), ER: Eritrea, GA: Gulf of Aden, K: Kenya, RS: Red Sea, S: Somalia, SA: Saudi Arabia, SP: Sudan plain, Y: Yemen. SeaWIFS image, courtesy NASA/JPL.

small fraction of their total length, may be related to their buoyancy in the crust (Lister and Kerr, 1991; Head and Wilson, 1992). Mafic dykes tend to propagate at a specific and theoretic crustal level called the level of neutral buoyancy (LNB). The top of mafic dykes may propagate at shallower depth and may locally erupt (Ryan, 1994).

The Ethiopian LIP (Fig. 1) is of great interest in the debate about lava flow feeding in LIPs. The Columbia Plateau dykes are clearly observed to be eruptive, but because the erosion is still weak they may not be representative of the whole swarm that should exist at depth. Precambrian to most Phanerozoic dyke swarms are observed after kilometres of crust have been eroded, so that the dominant flow is horizontal (e.g., Ernst and Baragar, 1992, for the 1.267 Ma Mackenzie dyke swarm; Callot et al., 2001, for a dyke swarm in the Tertiary North Atlantic Volcanic Province in Greenland). The dykes in this study, associated with the 30 Ma Ethiopian (Afar) plume, are observed in the Ethiopian lowlands west of the Abyssinian volcanic plateau at a depth of c. 1 km below the top of the plateau surface (Fig. 2). This exceptional geologic configuration is appropriate to study the relationships between the lava flows and the dykes, some of which are expected to be feeders while others are not. To distinguish between eruptive and non-eruptive dykes we use a mechanical approach based on fracture length distribution.

2. The studied dyke population

The study area is located in the lowlands region between the western edge of the Abyssinian volcanic plateau and the Ethiopian–Sudanese border (Fig. 1). Intense headward plateau erosion from the western Sudan eastward by the Blue Nile and its tributaries has removed a large fraction of the lava pile and left several outliers, one of which is Mount Belaya, southwest of Lake Tana (Fig. 3). Erosion has left the basal breccia of the trap series north of Mount Belaya, and removed the whole series to the south, where the outcropping terrain

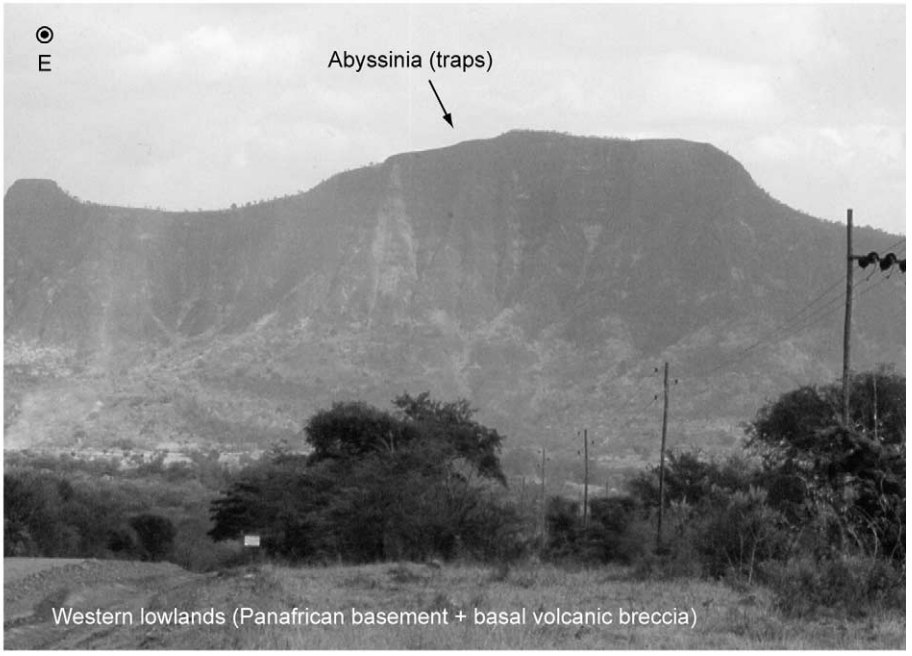

Fig. 2. Topographic setting of the dyke population area relative to the trap plateau. The dykes are observed c. 1000 m below the current top of the lava pile. The foreground displays a hilly morphology developed in Precambrian rocks. The hills are elongated and follow a Pan-African NE–SW shear zone fabric. Most of the dykes studied are aligned with this fabric but observed on the basal part of the trap series.

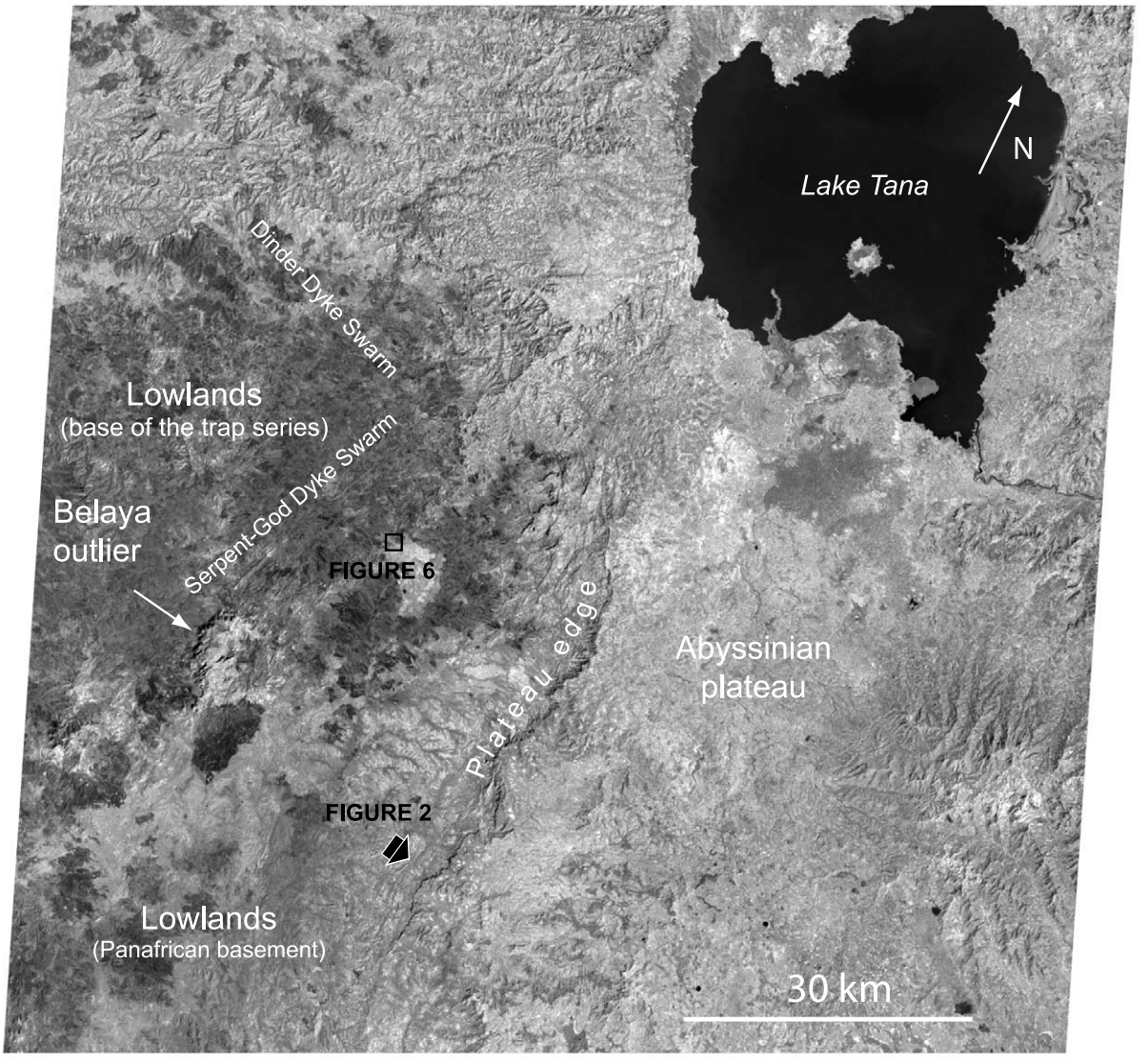

Fig. 3. Landsat ETM+ scene 170-02 (band 8) displaying the main features of the study area. The Serpent-God Dyke Swarm is clearly observed at the displayed scale owing to the prominent relief of silicic dykes (Fig. 4). The Dinder Dyke Swarm contains only basaltic dykes of no significant relief (Fig. 5) and is much less apparent in the figure. The top of the arrow locates the site where the photograph in Fig. 2 was taken and soars toward the direction of view. The black box locates the area displayed in Fig. 6. North toward the top.

is Pan-African basement. The studied dyke population is located between Lake Tana and Mount Belaya, and is made of basaltic and silicic dykes, with very few dykes of intermediate composition.

Some of the largest dykes in this region were identified in a geologic study of the Blue Nile basin by Jepsen and Athearn (1963) using aerial photographs and helicopter surveys, a swarm as such was reported by Mohr and Zanettin (1988) and Chorowicz et al. (1998) from interpretation of satellite imagery. Mège and Korme (2004) have combined field work and remote sensing data to examine the geologic setting of these dykes and showed that they follow pre-existing NE–SW and

NW–SE crustal weaknesses such as Precambrian shear zones. The silicic dykes appear to exclusively follow the NE–SW orientation. Dyke dating, analysis of magma crystallisation history, and flow characterisation are under way; nevertheless, several argon dating results have already been obtained, and have yielded ages in the order of 30 Ma ± a few hundred thousand years for both the basaltic and the silicic dykes, similar to the ages found for the traps in northern Ethiopia (Hofmann et al., 1997).

3. Analysis of dyke length distribution

3.1. Fracture population statistics

Dykes are magma-filled fractures and can therefore be analysed using tools developed for understanding the mechanical evolution of fracture populations. The length of fractures in a fracture population follows a power-law distribution (e.g., Gudmundsson, 1987; Scholz and Cowie, 1990; Scholz, 1997; Schultz, 2000) of the form

$$F = y\left(\frac{L}{L_{\max}}\right)^{-C} \quad (1)$$

where for a given fracture length L the number F of fractures of length $\geq L$ depends on the maximum fracture length $L_{\max}$, the population exponent C, and a coefficient y. Commonly, fracture distribution is analysed using a cumulative length–frequency plot.

For mechanically linked (en échelon) fractures, the length of the fracture that would be equivalent to the linked segments is

$$L = \sum 2a_i - \sum o_{i-j} \quad (2)$$

with $2a_i$ being the length of segment i and o_{i-j} the overlap between adjacent segments i and j.

3.2. Application to dykes

To our knowledge, the length distribution of a dyke fracture population has been reported in the literature (e.g., Gudmundsson, 1987) but not analysed in detail. Although dykes have the reputation to be mode I fractures, there are several reasons why dyke fractures might plot differently from other fractures, such as 'empty' mode I fractures.

Dyke propagation does not depend on the tectonic stress, lithostatic stress, and pore pressure solely, as other fractures do, it also depends on magma supply (Parfitt and Head, 1993) and on the balance between magma buoyancy and viscous pressure drop (e.g., Lister and Kerr, 1991).

Non-dyke fracture populations usually grow by gradual mechanical linkage of individual segments (e.g., Cowie and Shipton, 1998). In contrast, every dyke fracture grows instantaneously, and *independently* of the other dykes. Even though many dykes grow by several magma injections within the same conduit, dyke emplacement may be viewed as an instantaneous event because the injections must be very close in time in order for the dyke to remain a plane of preferred injection (Gudmundsson, 1995). When the magma supply has vanished for sufficiently long a time that the dyke has completely frozen, there is no reason that a new magma pulse should follow the previous dyke. The development of the new dyke is not influenced by the existence of the previous dyke. Thus, there is *no mechanical linkage* between the dykes.

It follows that dyke length distribution is akin to a pristine fracture length distribution. Analysis of dyke length distribution is therefore expected to provide a test to determine whether power-law distribution of fracture length in a population is an initial feature or builds gradually from a random initial distribution (Cladouhos and Marrett, 1996).

Moreover, there is evidence of a Precambrian shear zone (e.g., Vail, 1985) approximately parallel to the dykes in the study area. Therefore, this study is also a test as to the influence of crustal- or lithospheric-scale fabric and compositional anisotropy on power-law length distribution.

If a power law is a pristine feature of a fracture length distribution and is in addition insensitive to bedrock fabric, of particular interest will be how the likely coexistence of both eruptive and non-eruptive dykes affects the power law. Dyke fracture propagation occurs in response to magma overpressure in the feeding chamber. However,

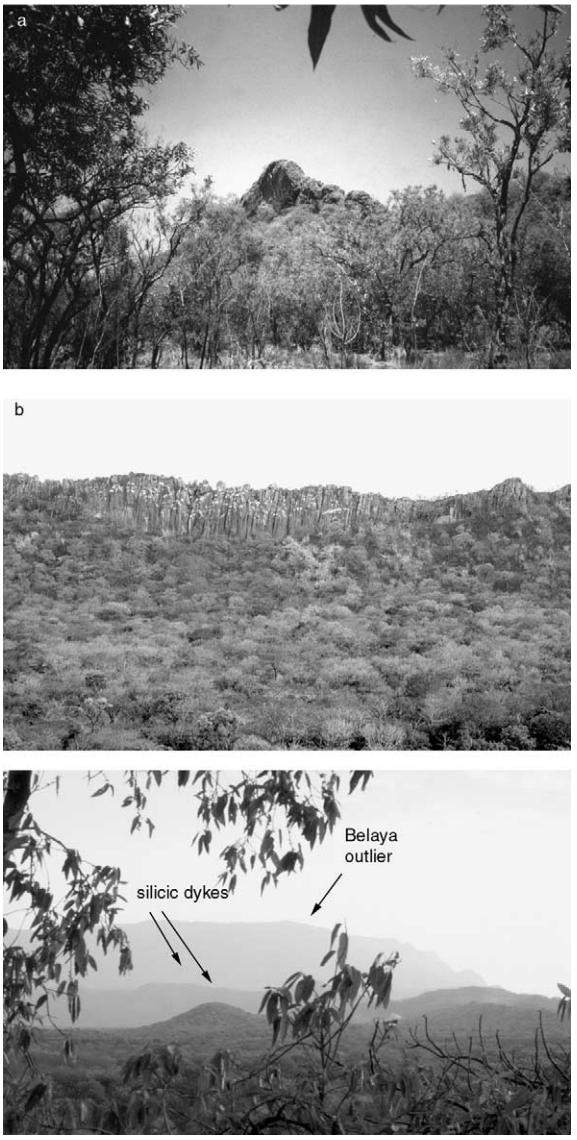

Fig. 4. Examples of silicic dyke exposures, which make some of the major topographic highs between the edge of the Abyssinian plateau and Sudan. (a) The Serpent-God Dyke, a microgranite-filled fracture that constitutes the thickest (20 m) and longest (30 km) dyke of the Serpent-God swarm (Mège and Korme, in press). At this location the dyke is 80–85°W-dipping and is surrounded by a debris slope several tens of metres high. (b) Another view of the Serpent-God Dyke northeast of panel a. The total elevation of the dyke and surrounding debris slope above the surrounding plain is c. 100 m. (c) Southwestward view of Mount Belaya and two silicic dykes from another silicic dyke.

when a dyke attains the surface, the chamber can depressurise without any, or with limited, increase of the dyke fracture length. Analysis of a dyke length distribution may thus reveal features reflecting the existence of both feeder and non-feeder dykes within the same swarm. This is expected for basaltic dykes, for which the LNB is below the topographic surface (Lister and Kerr, 1991; Ryan, 1994). Conversely, the density of silicic melts, $\sim$2200 kg/m^3, is less than the density of the most rocks, so that virtually every silicic dyke should be eruptive. Power-law distributions are a priori not expected to display anomalous features for silicic dykes.

3.3. Dyke sub-populations

Field work was carried out in 2000, 2001 and 2002. Exhaustive survey of the whole dyke swarm area is made difficult by dense vegetation cover and rarity of trails suitable for vehicles, most of which are not reported on topographic maps. Mège and Korme (in press) have identified two main dyke trends, NE–SW and NW–SE. Only exceptionally were the NW–SE dykes observed in the field due to the difficulty in accessing the areas where satellite images show that they are abundant. Many NE–SW dykes are of easier access and are within a one-day drive or two-day walk. Some are silicic but most are basaltic. Most are 80–90° dipping, although some segments of the thinnest basaltic dykes ($\leq$1 m) are observed to be 60° dipping.

Silicic dykes are observed as NE–SW-oriented ridges and can be easily identified because of their prominent topographic relief (Fig. 4). Most of them appear emerging from the northern slope of Mount Belaya. Thickness is in the range 4–20 m, with mean 9.9 m (Mège and Korme, in press). The dykes form thin ridge crests, surrounded by well-developed debris slopes that make most of the volume of the ridges. Ridge topography results from the strength contrast between silica-rich rocks and basaltic breccias in tropical morphoclimatic conditions.

The silicic dykes are parallel to numerous basaltic dykes. Because their lithology is similar to the lithology of the bedrock, the basaltic dykes

Fig. 5. Examples of basaltic dyke exposures. (a) Basaltic dyke 1.5–2 m thick in the Ayima River bed. (b) Basaltic dyke ~10 m wide observed as a low rocky lineament. Such dykes may be hard to identify in the field but appear as prominent features on satellite imagery or aerial photographs.

form no to very low relief (< 5 m). The thickness of those we observed in the field is in the range 0.5–9 m (mean 2.7 m), and is usually in the order of 1–5 m. The topographic contrast between silicic and basaltic dykes is thus enhanced by the fact that the silicic dykes are globally thicker than the basaltic dykes. Basaltic dykes are best observed across river beds (Fig. 5a). The largest ones frequently form small bumps and require careful observation to be identified. Some others are observed only as blocky linear patterns with almost no relief (Fig. 5b).

Field work has allowed the determination of dyke composition, and has allowed us to establish that the dykes observed to form topographic highs on imagery and topographic maps are silicic, whereas the others are basaltic. It also shows that most linear patterns observed on imagery are dykes, not tension fractures. These features are essential to the identification and characterisation of the dyke population. However, because of the difficulty in following dykes over long distances, and the difficulty in separating basaltic dykes and fractured portions of basaltic flows, field work has proved to be unhelpful in measuring dyke length.

Over the whole study area, we have used a Landsat ETM+ image (six multispectral channels, resolution 28.5 m/pixel; one panchromatic channel, 14.25 m/pixel; and one thermal infrared channel, 57 m/pixel), and orthophoto maps displaying Spot P photomosaics (one panchromatic channel, 10 m/pixel) overlain by a stereo-derived Spot digital elevation model. Lengths were measured on the Landsat ETM+ image and visually confirmed by checking on the Spot photomosaics.

The area is flat, which has allowed dyke length measurement at constant depth below the top of the trap series. In order to minimise measurement errors for short dykes imposed by image resolution, we did not consider dykes whose length is less than 1 km. Dykes that can be followed over a distance of several hundred metres were only considered if they were found to belong to an en échelon dyke according to the linkage criterion described in Section 4.

The error in dyke length due to image resolution is thought to be negligible. Due to dyke relief, which can be observed on satellite imagery and digital elevation models, most silicic dykes are clearly observed to stop along strike at the location where they actually stop on the ground (the reference structural depth). Basaltic dykes are rarely more than a few metres thick and their end zone along strike is probably less than a few pixels. Due to linear scaling of dyke length and thickness (e.g., Gudmundsson, 1990), the error on dyke length that may exist if measured using satellite imagery at constant resolution (here the resolution of Landsat ETM+) is thus a small and systematic error that may affect the coefficient of the

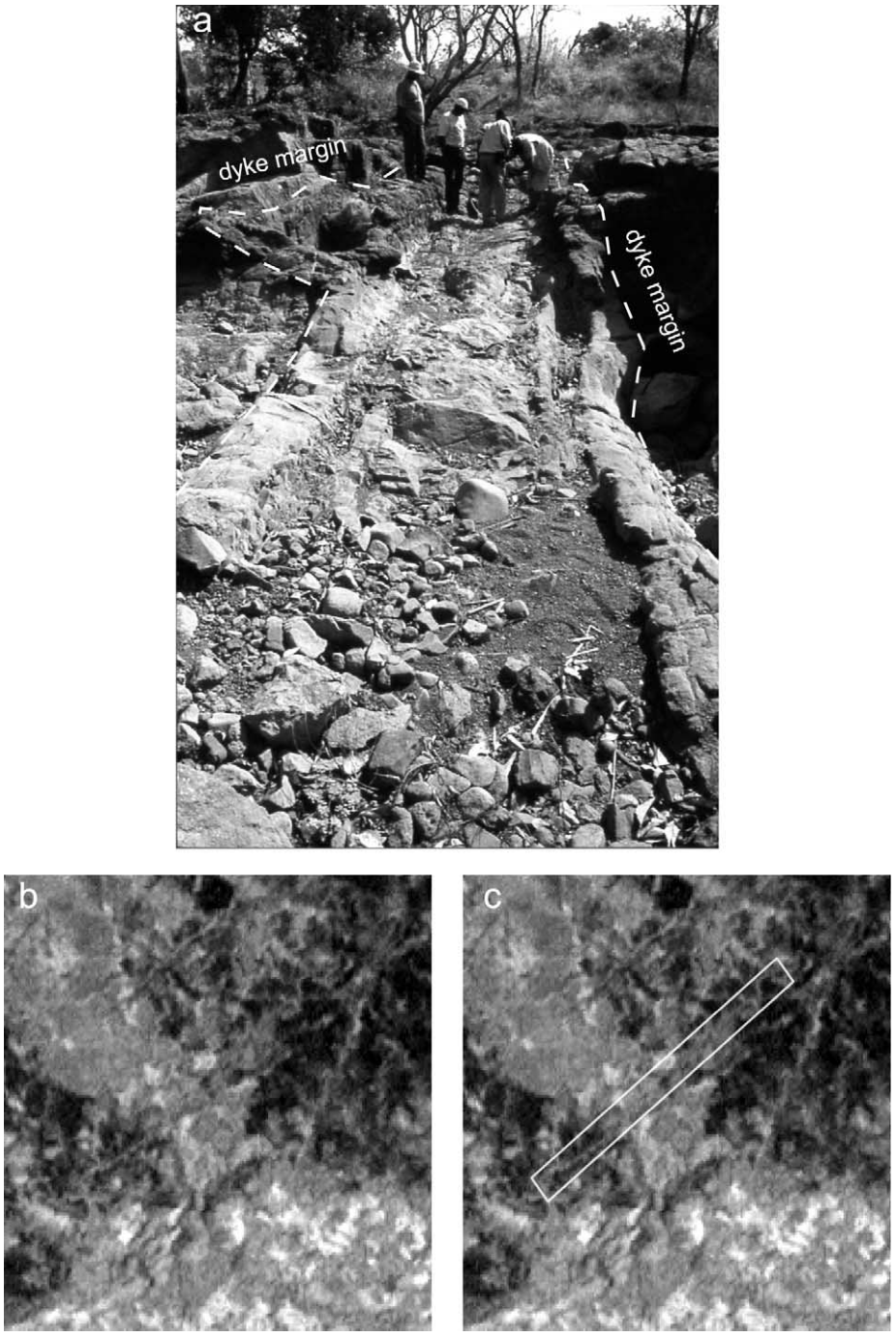

Fig. 6. Basaltic dyke observed in a dry river bed west of Jawi village. (a) Field photograph., (b) Landsat panchromatic image (14.25 m, location in Fig. 3). (c) The same image with the dyke outlined. Dyke thickness is 2 m (foreground) to 3 m (background), but is observed on the Landsat ETM+ panchromatic image (14.25 m/pixel) because of its morphology and influence on surrounding vegetation.

dyke fracture population (y in Eq. 1) but not its exponent (C).

Satellite imagery is appropriate to identify dykes some of which are thinner than the pixel size. This is because in addition to their own width, many dykes influence the reflectance of surrounding areas, by way of composition contrasts, topography, morphology, and vegetation changes. Dykes having a positive topography are surrounded by fallen blocks and weathering products that have a different reflectance than the country rock. Vegetation may also change in the dyke vicinity because the dykes are major water circulation vectors. For instance, the dyke in Fig. 6 is only 2–3 m thick, and on a Landsat colour composite image of resolution 28.5 m it is observed as a one-pixel-wide lineament. At 14.25 m resolution it alters country rock reflectance over three pixels and can be easily identified.

Every dyke observed in the field whose thickness exceeds a couple of metres was also observed on satellite imagery. However, conversely, not all the dykes inferred from satellite imagery have been observed to correspond to any linear trend in the field. This is a well-known feature for geologic mappers who use remote sensing images (Zimbelman, 2001), who have noted that improving data resolution does not systematically result in improvement in science interpretation. Perhaps all the dykes that can be observed on imagery could have been observed if they had been specifically looked for, but part of the imagery was not available during the field survey, and it is likely that many basaltic dykes were missed due to the bad outcropping conditions (e.g., Fig. 5b). Therefore, for identifying dykes and determining their length, satellite imagery was found to be more reliable than field data.

An array of dyke segments that are disconnected at the observed structural level but belong to the same fracture according to some mechanical linkage criterion are defined as en échelon dyke segments. Dyke *segments* are defined as individual, disconnected dyke exposures that may

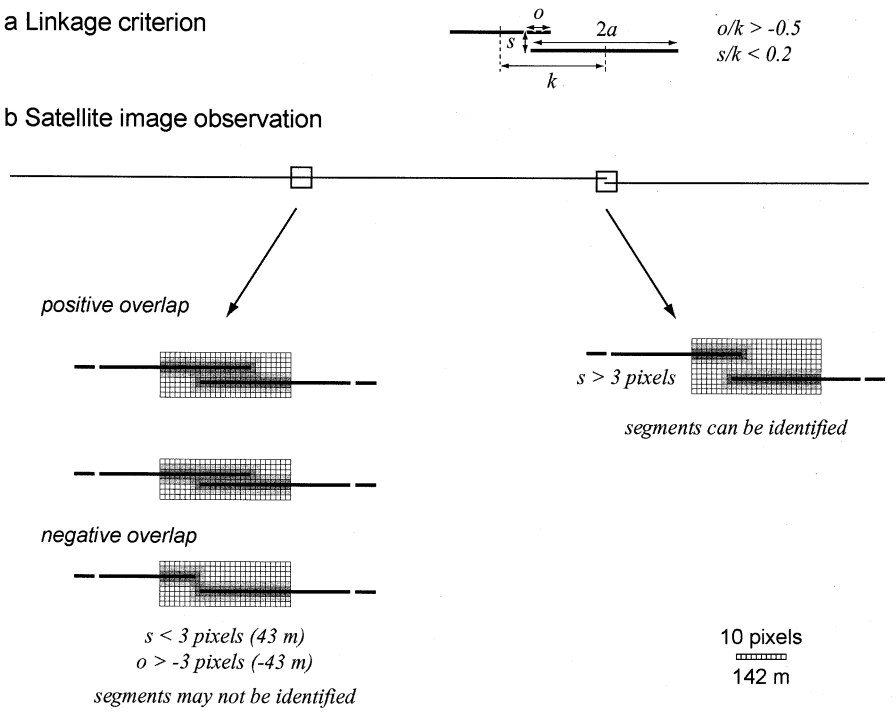

Fig. 7. (a) Linkage criterion used to determine en échelon dyke segments. (b) Influence of relay zone size on identification of segment tip.

or may not display an en échelon arrangement. *Independent* dykes refer to continuous dyke exposures that are not mechanically linked with other dyke outcrops.

In order for a dyke population to be analysed, en échelon dyke segments and other dyke segments must be identified and separated as distinctly as possible, because the segments of an en échelon dyke must be replaced by a single dyke whose length is the cumulated length of its segments. Because of vegetation and erosion, field evidence of disconnected segments belonging to the same dyke, such as provided by horn geometry, was never found. Evidence for mechanical linkage has been determined on satellite imagery using a criterion identified by Schultz (2000) from comparing mechanically linked and unlinked fracture data sets. Two en échelon fracture segments are mechanically linked if segment overlap o ($o < 0$ for segment underlap), across-strike separation s, and distance k between mid-points adjacent segments are related so that

$$o/k > -0.5 \text{ and } s/k < 0.2 \quad (3)$$

All three parameters required in these equations can be determined in map view. Eq. 3 helps identify mechanically linked segments of en échelon dykes at the considered structural depth (current topographic surface). It is important to note that two dyke segments that are found to be unlinked at the surface using Eq. 3 may be connected at depth to the same dyke body. Mechanically, however, at the surface level, the growth of one segment is not influenced by the growth of the other.

Eq. 3 also helps determine whether or not the error induced by mapping small dyke segments as a single continuous dyke owing to the image resolution issue is significant for dyke population analysis. Given that the smallest dykes considered are three pixels thick at least, dyke segments up to ~40 m apart may appear on the Landsat 7 panchromatic image as if they were a single segment (Fig. 7). At relay size approaching Landsat 7 panchromatic resolution, the minimum k, k_{min}, for the two segments to be linked never exceeds 175 m (Fig. 8). If the length of the overlap zone is small compared with the segment length $2a$, then $2k$ is of the same order as $2a$, and larger than $2k_{min} = 350$ m. This is typically the case for en échelon (linked) fractures, because the segment tips are deflected toward each other during segment growth, and the two segments merge before the length of the overlap has much increased (e.g., Cartwright et al., 1995). Overlaps where $2k$ is significantly smaller than $2a$ and may be smaller than $2k_{min}$ are most likely due to two parallel dykes that are not genetically linked. Such dykes cannot be clearly separated, and failure to identify

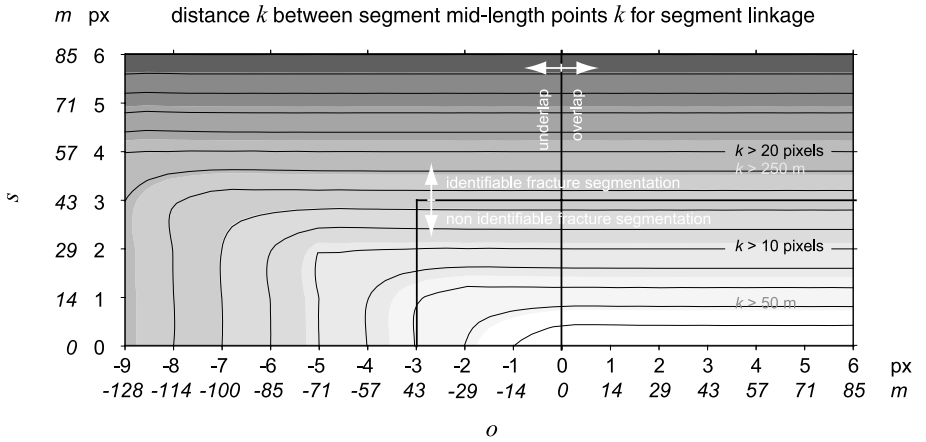

Fig. 8. Minimum distance between segment mid-length points (k) for segment linkage as a function of segment overlap (o, negative for underlap) and segment separation (s). Black curves and labels in pixels, grey shades and labels in metres. The bottom right part of the graph shows k for segment proximity approaching Landsat 7 band 8 image resolution, in which case the linkage interpretation is hard to determine.

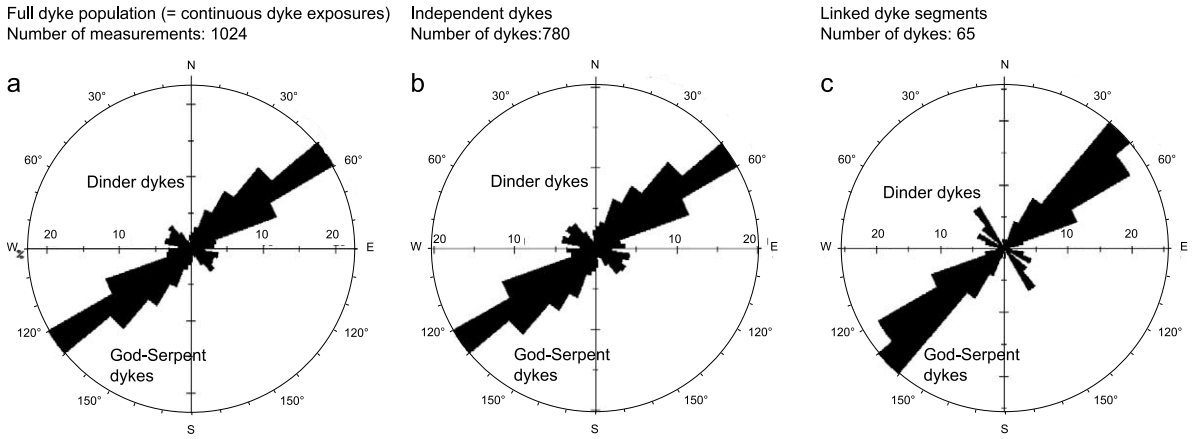

Fig. 9. Dyke orientation and segmentation in the Tana–Belaya area. The horizontal graduations give the percentage of data within 10°-wide classes. (a) Every dyke and dyke segment is plotted as a single fracture. (b) Only the independent dykes are plotted. (c) Only the en échelon dykes are plotted. All the dykes reported on this figure were identified and measured using Landsat ETM+ and Spot imagery.

those of length >1 km (the minimum dyke length considered in this study) may bias the dyke length distribution. We assume, however, that such a case should be infrequent, because (1) there is statistically not more chance for a dyke to intrude at a very short distance from another, frozen dyke, than at greater distance; (2) if dyke intruded earlier is not totally frozen, a new propagating dyke may be trapped in it because it is a weakness zone, but has little chance to intrude the host rock at a short distance from the first dyke, because the compressive stress induced by the first dyke in the host rock around it (e.g., Pollard et al., 1983) should build a shadow zone for new dyke propagation, for a period of time depending on the magnitude of the tectonic stress. Cases where two unlinked dyke segments are counted as a single dyke are thus thought not to influence dyke length distribution significantly. Most unseen dyke segmentation is thought to correspond to unseen en échelon dyke segments. They are thus correctly, though implicitly, accounted for during the length measurement process.

4. Results

There were 1024 dyke exposures measured. Based on en échelon geometry identification, the

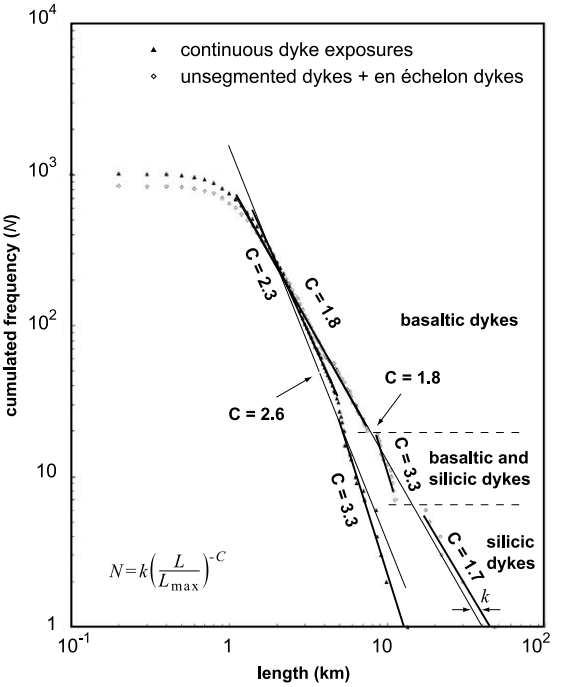

Fig. 10. Length-cumulated frequency plot for the dykes in the Tana–Belaya area. The diamonds are for a population in which dyke segmentation is taken into account, whereas the filled triangles are for the population of continuous dyke exposures. The straight lines represent power-law fits to the populations. Thin lines are for the whole populations, which have exponent C as indicated horizontally. The thick lines are fits for the sub-populations discussed in the text. The exponents C for the sub-populations are given along the lines.

number of independent dykes was found to be 780, and the number of en échelon dykes was found to be 65 (Fig. 9). The mean length of all the continuous dyke exposures is 1.6 km, and if the en échelon dykes are counted as single dykes, then the mean length increases by less than 100 m. The longest dyke, also that of globally highest elevation, is the NE–SW silicic Serpent-God Dyke (Fig. 4). It displays ~30 major en échelon segments of accumulated length 48 km. The segments in the northernmost 15 km of the dyke display a curved geometry that may reflect reorientation of stress trajectories. The longest dyke in the NW–SE swarm is 23 km long and, from its topography, of probably basaltic composition. The accumulated dyke length for the whole swarm is only 1650 km, which corresponds to the length of only one to five dykes in typical giant dyke swarms in other LIPs (Ernst et al., 2001). It is less than the length of some single giant dykes in the Mackenzie swarm.

Two dyke populations were plotted, depending on whether en échelon dyke geometry is taken into account (Fig. 10). Whatever the population, dyke length follows a power-law distribution. This solves two issues raised earlier. Not only is a power-law distribution an initial feature of the fracture distribution, but also the basement anisotropy resulting from large-scale structures and compositional variations does not significantly affect the dyke length distribution. Interpretation of dyke population statistics in terms of common fracture population statistics is thus strongly grounded.

As the topographic surface depth below the initial trap surface is unrelated to the dyke emplacement mechanism, the power-law distribution obtained would likely be observed at any other structural level above the magma reservoir. Although dyke segment linkage does depend on the structural level considered, the overall distribution law pattern is expected to be preserved at any structural level considered.

Accounting for mechanical linkage of en échelon dykes very significantly affects the exponent, which decreases from $C=2.6$ to $C=1.8$ (Fig. 10). Linkage also increases the correlation coefficient, which is good for both populations but even better when dyke segmentation is taken into account (0.994 v. 0.970).

The exponent $C=1.8$ is similar to the exponent Segall and Pollard (1983) obtained for tens of metres long mode I cracks. This value is in the main range of exponents for fracture populations, for which the lower and upper bounds reported in the literature are $C=0.6$ and $C=2.9$ (Jackson and Sanderson, 1992; Cladouhos and Marrett, 1996; Schultz, 2000). The highest exponents are found in regions where outcropping conditions make it difficult to interpret mechanical fracture linkage (Cladouhos and Marrett, 1996). For the dyke fracture population in which dyke segmentation was not accounted for, similarly, the high exponent $C=2.6$ is explained by a mechanical shortcoming.

The curved shape of the cumulative frequency distribution at the short end of the distribution (Fig. 10) is a classical feature ascribed to a mapping bias (Jackson and Sanderson, 1992). In the Tana–Belaya area this bias partly results from approaching the pixel size. Small lineaments may usually be interpreted in different ways, as fractures, erosional scarps, anthropic tree alignments, etc. Thus, the length distribution in Fig. 10 is thought not to be reliable below ~1 km.

The dyke population that does not account for dyke segmentation displays a falloff at mid-distribution. The overall distribution may be approximated by two power-law fits instead of one, with exponents $C=2.3$ and $C=3.3$ for the shortest and longest dyke sub-populations, respectively. Both exponents are high, which affects the reliability of the plot.

The slope break is no longer apparent in the dyke population that accounts for en échelon dykes, the exponent of which also globally decreases. The distribution of the dyke population accounting for en échelon segments is divided into three parts. At short length the power-law exponent for the whole population, $C=1.8$, provides a very good fit to the distribution. At 9–10 km, the distribution is shifted upward (or rightward), meaning that the number of dykes more than ~10 km long is unusually high. At intermediate lengths (right of the distribution shift) the distribution slope increases abruptly to $C=3.3$ until

10–20 km. This slope increase cannot be ascribed to data censoring (when the size of some fractures exceeds the size of the sampling window, Jackson and Sanderson, 1992) since this sub-population does not end the distribution. A larger distribution shift occurs at 10–20 km, after which the distribution slope goes back to a lower value ($C = 1.7$). The coefficient k for this sub-population is slightly higher than that of the whole distribution and the short length sub-population.

The dyke distribution patterns described above are correlated with dyke lithology because dyke length is partly correlated with composition. The longest dykes are essentially all silicic. They make up most of the dyke sub-population of slope 1.7 in Fig. 10. A few of them enter the intermediate sub-population (slope 3.3), and a very few of them are in the sub-population that includes the short dykes (slope 1.8).

An explanation for the observed variations in population distribution is given in Fig. 11. A basaltic dyke whose propagation is not impeded by waning magma supply (Parfitt and Head, 1993) may grow and build a magma pressure that is large enough to cut across the zone where its density equals the density of the host rock, and propagate up to the surface. When the dyke erupts, it begins depressurising more rapidly than it would do if it was non-emergent. The dyke propagation speed decreases and the dyke eventually stops before it has attained the length it would have had if it was not a feeder dyke. The volume of the erupted magma is a measure of the magma volume that *would have* contributed, but *did not* contribute to increasing the dyke dimensions. On a length-cumulated frequency plot, for a given magma reservoir, there is a critical length below which the dykes are too small to be eruptive and above which they attain the topographic surface. The topographic surface traps the length of the eruptive dykes at this critical length, which marks a plateau in the distribution (Fig. 11a). Since all the

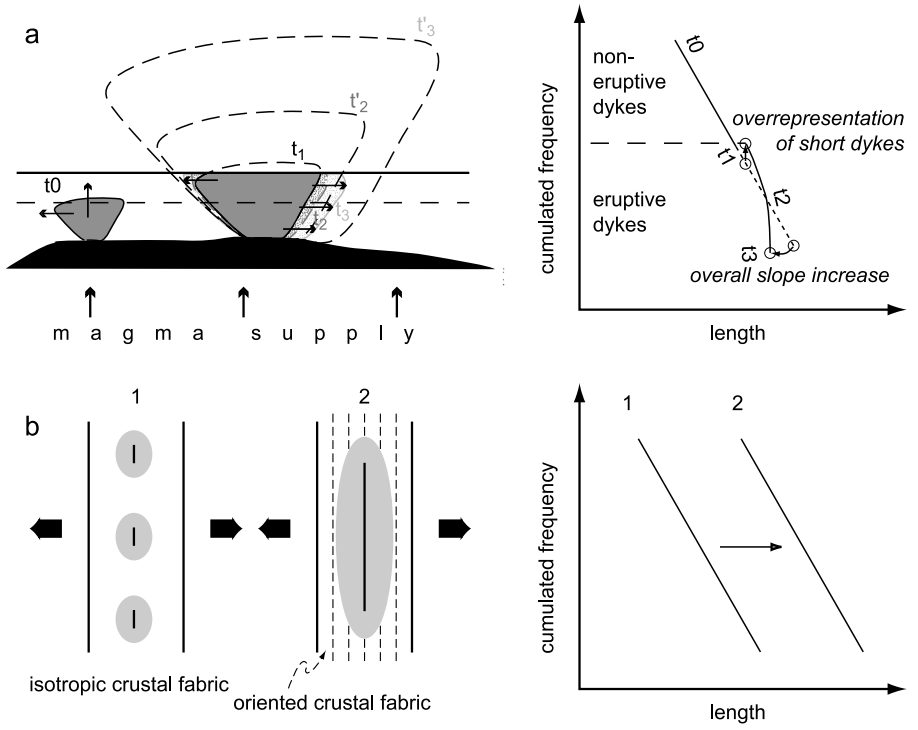

Fig. 11. Explanation for the distribution anomalies observed in the population accounting for dyke segmentation. (a) Influence of the free surface on population distribution. (b) Influence of changing magma reservoir geometry owing to oriented crustal fabric during crustal stretching on the distribution of the silicic dyke population.

dykes of length greater than this critical length are eruptive, they will all depressurise abruptly and their propagation will suddenly slow down and stop, resulting in distribution curtailment for the dykes above the critical length (Fig. 11a). This interpretation is supported by the inference from the elevation of the surrounding plateau and Belaya Mountain that the topographic surface may have been up to ~1500–2000 m higher when the dykes were emplaced, i.e., not far from the neutral buoyancy zone in the crust for mafic dykes (Wilson and Head, 1994). At such a depth, the vertical propagation of the narrowest and least pressurised dykes slows down and stops, whereas the largest ones have enough internal pressure to attain the surface and erupt.

Owing to the positive buoyancy of silicic dykes over the whole crust up to the surface, they propagate more vertically and less horizontally than basaltic dykes, and all of them should attain the surface and erupt, provided that the magma supply rate is sufficiently high. Silicic domes are observed in various areas on the Abyssinian volcanic plateau (Ayalew and Yirgu, 2003). Some of them are aligned with the NE–SW dyke swarm, and might result from the eruption of similarly oriented dykes (work in progress). Thus, in contrast to basaltic dykes, the population of silicic dykes is expected not to display a slope break similar to that observed for the basaltic dykes. The power-law exponent for silicic dykes is expected to be of the same order as the exponent of other fracture populations. Fig. 10 indeed shows a small difference between the basaltic and silicic dyke sub-population exponents (1.7 v. 1.8).

However, owing to their larger component of vertical versus horizontal propagation, at similar supply rates, the dykes from the silicic population are also expected to be shorter than the basaltic dykes. The population coefficient y should thus be smaller for the silicic dyke population. That is in contradiction to the results reported in Fig. 10, where y is larger for the silicic dykes (Fig. 11). We suggest that a possible explanation is related to the change in reservoir geometry with time during regional tectonic extension. The silicic dykes may have been emplaced from the same reservoir as the basaltic dykes after differentiation occurred, or from a distinct crustal reservoir aligned with the basaltic reservoir. Geochronological and geochemical analyses are in progress and will help assess these hypotheses. In both cases, silicic dyke dilation during crustal stretching parallel to the NE–SW Pan-African shear zone should have increased the chamber aspect ratio (Fig. 11b). Silicic dykes may account for as much as half the dilation in the studied area (Mège and Korme, in press), which supports the idea that the reservoir may have extended beyond the extent it had when the basaltic dykes were emplaced. Therefore, when the silicic dykes were emplaced, the rupture at the top of the reservoir along its major horizontal axis may have been longer than when the basaltic dykes were emplaced. Initially, the dykes would leave the reservoir with a greater length, resulting in a higher power-law coefficient in the distribution.

5. Synthesis

The dyke length distribution correlates excellently with a power-law fit, even when dyke en échelon segments are counted as individual, independent dykes. However, in that case, the high exponent for this population suggests that this statistical result may not be geologically acceptable. When the en échelon dyke segments of a given dyke are assembled, the exponent decreases to a typical value for other fracture types, 1.8. A distribution shift at 9–10 km, associated with a steeper slope (3.3) for longer dykes, is ascribed to a transition from non-eruptive to eruptive basaltic dykes. All the silicic dykes are thought to have been eruptive owing to their positive buoyancy throughout the crust. Due to this homogeneous propagation behaviour, this sub-population displays an exponent typical of fracture populations (1.7) without any slope break. The latter result is, however, to be considered with caution because the silicic dyke sub-population is much smaller than the basaltic dyke sub-population.

Whether other dyke populations will display clues to eruptive dykes will depend on several factors. Firstly, en échelon dyke segments need to be identified using an appropriate method to

ensure that the structural interpretation of the results is reliable. Secondly, the observation level should lie between the level of neutral buoyancy and the surface, in order to make sure that some dykes will stay within the crust while others will erupt. Thirdly, the dyke length range in the distribution must start with dykes as small as possible in order for the power law to account primarily for small and non-eruptive dykes, which will constitute the homogeneous reference population, and highlight the eruptive dykes as a population that departs from the non-eruptive population. Fourthly, in order to interpret the discrepancy between the power law and the eruptive dykes, the influence of other factors inducing length curtailment at the upper bound of the distribution, including data censoring and major rheologic discontinuities, should be determined carefully. Dyke fracture length statistics is a promising topic for the identification of feeder dykes in intensely eroded areas and needs to be further investigated using additional data sets.

Acknowledgements

This work was funded by a cooperation agreement between Pierre and Marie Curie University and Addis Ababa University and the CNRS/INSU *Intérieur de la Terre* programme. Paul Mohr is thanked for critical reading of the initial manuscript, and Henry Halls and Editor Lionel Wilson for helping clarify its objectives.

References

Ayalew, D., Yirgu, G., 2003. Crustal contribution to the genesis of Ethiopian plateau rhyolitic ignimbrites: basalts and rhyolite geochemical provinciality. J. Geol. Soc. London 160, 47–56.

Cadman, A.C., Tarney, J., Baragar, W.R.W., Wardle, R.J., 1994. Relationship between Proterozoic dykes and associated volcanic sequences: evidence from the Harp Swarm and Seal Lake Group, Labrador, Canada. Precamb. Res. 68, 357–374.

Callot, J.-P., Geoffroy, L., Aubourg, C., Pozzi, J.P., Mège, D., 2001. Magma flow in shallow dykes from the E-Greenland margin inferred from magnetic fabric studies. Tectonophysics 334, 313–329.

Cartwright, J.A., Trudgill, B.D., Mansfield, C.S., 1995. Fault growth by segment linkage: an explanation for scatter in maximum displacement and trace length data from the Canyonlands Grabens of SE Utah. J. Struct. Geol. 17, 1319–1326.

Chorowicz, J., Collet, B., Bonavia, F.F., Mohr, P., Parrot, J.-F., Korme, T., 1998. The Tana basin, Ethiopia: Intraplateau uplift, rifting and subsidence. Tectonophysics 295, 351–367.

Cladouhos, T.T., Marrett, R., 1996. Are fault and linkage models consistent with power-law distributions of faults lengths? J. Struct. Geol. 18, 281–293.

Cowie, P.A., Shipton, Z.K., 1998. Fault tip displacement gradient and process zone dimensions. J. Struct. Geol. 20, 983–997.

Ernst, R.E., Baragar, W.R.A., 1992. Evidence from magnetic fabric for the flow pattern in the Mackenzie giant radiating dyke swarm. Nature 356, 511–513.

Ernst, R.E., Buchan, K.L., 1997. Giant radiating dyke swarms: Their use in identifying Pre-Mesozoic large igneous provinces and mantle plumes. In: Mahoney, J.J., Coffin, M.F. (Eds.), Large Igneous Provinces: Continental, Oceanic, and Planetary Flood Volcanism. AGU Geophys. Monogr. 100, 297–333.

Ernst, R.E., Grosfils, E.B., Mège, D., 2001. Giant dyke swarms: Earth, Venus and Mars. Annu. Rev. Earth Planet. Sci. 29, 489–534.

Fruchter, J.S., Baldwin, S.F., 1975. Correlations between dikes of the Monument swarm, Central Oregon, and Picture Gorge basalt flows. Geol. Soc. Am. Bull. 86, 514–516.

Fuller, R.E., 1927. The closing phase of a fissure eruption. Am. J. Sci. 14, 228–230.

Gudmundsson, A., 1987. Geometry, formation and development of tectonic fractures on the Reykjanes Peninsula, Southwest Iceland. Tectonophysics 139, 295–308.

Gudmundsson, A., 1990. Emplacement of dikes, sills and crustal magma chambers at divergent plate boundaries. Tectonophysics 176, 257–275.

Gudmundsson, A., 1995. The geometry and growth of dykes. In: Baer, G., Heimann, A. (Eds.), Physics and Chemistry of Dykes. Balkema, Rotterdam, pp. 23–34.

Head, J.W., III, Wilson, L., 1992. Magma reservoirs and neutral buoyancy zones on Venus: implications for the formation and evolution of volcanic landforms. J. Geophys. Res. 97, 3877–3903.

Hofmann, C., Courtillot, V., Féraud, G., Rochette, P., Yirgu, G., Ketefo, E., Pik, R., 1997. Timing of the Ethiopian flood basalt event and implications for plume birth and global change. Nature 389, 838–841.

Hooper, P.R., 1997. The Columbia River flood basalt province: Current status. In: Mahoney, J.J., Coffin, M.F. (Eds.), Large Igneous Provinces: Continental, Oceanic, and Planetary Flood Volcanism. AGU Geophys. Monogr. 100, 1–27.

Jackson, P., Sanderson, D.J., 1992. Scaling of fault displacements from the Badajoz-Córdoba shear zone, SW Spain. Tectonophysics 210, 179–190.

Jepsen, D.H., Athearn, B.M.J., 1963. General Geology Recon-

naissance Map, Vicinity of Ismale Georgis. Ethiopian Department of Water Research, Addis Ababa, 5.2-LT-3.

Lister, J.R., Kerr, R.C., 1991. Fluid-mechanical models of crack propagation and their application to magma transport in dykes. J. Geophys. Res. 96, 10,049–10,077.

Mège, D., Korme, T., 2004. Dyke swarm emplacement in the Ethiopian Large Igneous Province: not only a matter of stress. J. Volcanol. Geotherm. Res., in press (doi: 10.1016/S0377-0273(03)00318-4).

Mohr, P., 1963. The Ethiopian Cainozoic lavas, A study of some trends: spatial, temporal, and chemical. Bull. Geophys. Observ. Addis Ababa 6, 103–144.

Mohr, P., Zanettin, B., 1988. The Ethiopian flood basalt province. In: McDougall, J.D. (Ed.), Continental Flood Basalts. Kluwer Academic, Dordrecht, pp. 63–110.

Parfitt, E.A., Head, J.W., III, 1993. Buffered and unbuffered dike emplacement on Earth and Venus: Implications for magma reservoir size, depth, and rate of magma replenishment. Earth Moon Planets 61, 249–281.

Peulvast, J.P., 1991. Structural geomorphology and morphotectonic evolution of an uplifted rifted margin, the Scoresby Sund area, East Greenland. Z. Geomorphol. 82, 17–34.

Pollard, D.D., Delaney, P.T., Duffield, W.A., Endo, E.T., Okamura, A.T., 1983. Surface deformation in volcanic rift zones. Tectonophysics 94, 541–584.

Reidel, S.P., Tolan, T.L., Hooper, P.R., Beeson, M.H., Fecht, K.R., Bentley, R.D., Anderson, J.L., 1989. The Grande Ronde basalt, Columbia River Basalt Group; stratigraphic descriptions and correlations in Washington, Oregon, and Idaho. In: Reidel, S.P., Hooper, P.R. (Eds.), Volcanism and Tectonism in the Columbia River Flood-Basalt Province. Geol. Soc. Am. Spec. Pap. 239, 21–53.

Ryan, M.P., 1994. Neutral-buoyancy controlled magma transport and storage in mid-ocean ridge magma reservoirs and their sheeted-dike complex: a summary of basic relationships. In: Ryan, M.P. (Ed.), Magmatic Systems. Academic Press, New York, pp. 97–138.

Scholz, C.H., 1997. Earthquake and fault populations and the calculation of brittle strain. Geowissenschaften 15, 124–130.

Scholz, C.H., Cowie, P.A., 1990. Determination of total strain from faulting using slip measurements. Nature 346, 837–839.

Schultz, R.A., 2000. Fault-population statistics at the Valles Marineris Extensional Province, Mars: implications for segment linkage, crustal strains, and its geodynamical development. Tectonophysics 316, 169–193.

Segall, P., Pollard, D.D., 1983. Joint formation in granitic rock of the Sierra Nevada. Geol. Soc. Am. Bull. 94, 563–575.

Swanson, D.A., Wright, T.L., Helz, R.T., 1975. Linear vent systems and estimated rates of magma production and eruption of the Yakima basalt on the Columbia Plateau. Am. J. Sci. 275, 877–905.

Tolan, T.L., Reidel, S.P., Beeson, M.H., Anderson, J.L., Fecht, K.R., Swanson, D.A., 1989. Revisions to the estimates of the areal extent and volume of the Columbia River Basalt Group. In: Reidel, S.P., Hooper, P.R. (Eds.), Volcanism and Tectonism in the Columbia River Flood-Basalt Province. Geol. Soc. Am. Spec. Pap. 239, 1–20.

Vail, J.R., 1985. Pan-African (late Precambrian) tectonic terrains and the reconstruction of the Arabian-Nubian shield. Geology 13, 839–842.

Waters, A.C., 1961. Stratigraphic and lithologic variations in the Columbia river basalt. Am. J. Sci. 259, 583–611.

Wilson, L., Head, J.W., III, 1994. Mars: review and analysis of volcanic eruption theory and relationships to observed landforms. Rev. Geophys. 32, 221–263.

Zimbelman, J.R., 2001. Image resolution evaluation of genetic hypotheses for planetary landscapes. Geomorphology 37, 179–199.